AIAA JOURNAL
Vol. 34, No. 3, March 1996

# Infrared Emission from High-Temperature $H_2O(\nu_2)$: A Diagnostic for Concentration and Temperature

T. E. Parker*
*Colorado School of Mines, Golden, Colorado 80401-1887*
and
M. F. Miller,† K. R. McManus,† M. G. Allen,‡ and W. T. Rawlins§
*Physical Sciences, Inc., Andover, Massachusetts 01810*

**A shock tube system was used to produce known concentrations of water at combustion temperatures so that the infrared radiance from a portion of the $H_2O(\nu_2)$ band could be measured as a function of temperature and wavelength. The resulting data set was used to determine the efficacy of a spectral emission diagnostic for $H_2O$ temperature and column density at the exit plane of a supersonic combustor. Temporally and spectrally resolved, optically thin infrared emission, at 13 wavelengths between 6.5 and 9.5 $\mu$m, was observed from shock-heated $H_2O/N_2$, $H_2/O_2/N_2$, and $H_2/O_2$/Ar mixtures, at pressures of 1 and 5 atm and temperatures between 1400 and 3000 K. Least-squares analysis of the temperature-dependent intensities for each wavelength channel gave parameters that accurately describe the radiance as a function of wavelength and temperature over the entire temperature range of the measurements. The accuracy to which temperatures and $H_2O$ column densities can be determined from these parameters was then estimated. Radiometric data were compared with predictions from a widely used band model, corrections for optically thick systems were explored, and the relationship between optically thin radiance and the optical cross section produced. Column densities at which corrections for optical thickness are required were also calculated.**

## Introduction

THE development of high-speed propulsion systems (e.g., scramjets) requires measurements of important flowfield parameters such as temperature, pressure, and velocity to evaluate performance and verify computational models. However, scramjet flows typically are 1000–3000 K in temperature with velocities of 2 km/s or more. Clearly this is a very difficult measurement environment, and the combination of temperature and velocity mandate a diagnostic set that is nonintrusive in nature. Previous investigations have focused on the mixing zone and have demonstrated the utility of planar laser imaging techniques, such as planar laser-induced fluorescence.[1–4] Additionally, emission measurements have been used to monitor inlet flow properties in high-enthalpy flow facilities.[5] However, diagnostics specifically focused on the exit plane to quantify product formation ($H_2O$) and flow temperature are required to monitor overall scramjet performance. Previous investigations have attempted to apply fluorescence detection to $H_2O$, but quantitative interpretation of the fluorescence is complicated by the electronic energy state structure of the molecule.[6–8] Laser-based absorption measurements of water have also been developed.[9,10] These measurements can be very accurate but in many cases do not provide suitable time resolution and can be relatively hardware intensive. As an alternative to active or laser-based measurements, passive emission from water can be used to quantify both the flow temperature and water concentration within a high-speed flow. This technique is the focus of this paper.

Previous work at Physical Sciences[11,12] has reported preliminary observations of spectrally resolved infrared emission from combustion-generated $H_2O$ at the exit plane of a shock tunnel with interpretation based upon a limited database from shock tube observations of shock-heated $H_2O$.[11] A more comprehensive database is used in this paper, which describes results of a comprehensive shock tube investigation of the $H_2O(\nu_2)$ band strength as a function of wavelength and temperature, using both shock-heated and combustion-generated $H_2O$. Data from the shock tube measurements have been analyzed to generate a set of empirical fitting functions, which can be used to determine temperatures and column densities from observations of infrared emission in the combustor exit plane. Uncertainties in the empirical database because of measurement and calibration error as well as uncertainties in calculated system properties defines the accuracy of the exit plane temperature and $H_2O$ column density determinations.

The emission based measurement for $H_2O$ utilizes thermal infrared emission from a portion of the bend-mode ($\nu_2$) rotational-vibrational band centered at 6.27 $\mu$m. This band was chosen over the stronger $\nu_3$ band near 2.7 $\mu$m to avoid spectral interference from the vibrational bands of OH ($\Delta v = 1$) and NO ($\Delta v = 2$). Although a small overlap of the short-wavelength portion of the $\nu_2$ band and the long-wavelength tail of the NO ($\Delta v = 1$) 5.3 $\mu$m band exists, comparison of emission data for NO (Ref. 5) with that for $H_2O$ reveals that interference from NO at wavelengths greater than 6.5 $\mu$m is negligible. $NO_2$ also radiates in this spectral region but will not be present at combustion temperatures. Thus we have chosen the wavelength region 6.50–9.44 $\mu$m for the combustor $H_2O$ diagnostic. The measurement technique uses a HgCdTe array spectrometer to observe spectrally resolved $H_2O(\nu_2)$ emission between 6.50 and 8.55 $\mu$m, and a bandpass-filtered HgCdTe radiometer to observe emission at 9.44 $\mu$m. This combination probes the P-branch and vibrational hot bands of the $\nu_2$ system and the pure-rotation transitions of $H_2O$. The relative bandshape in the spectral region changes with temperature (the relative radiance at longer wavelengths increases), whereas the total intensity is sensitive to both temperature and $H_2O$ column density. Thus measurements of intensity ratio at two or more well-separated wavelengths can be used to define the temperature of the radiating $H_2O$, and once this temperature is known, absolute intensity at a given wavelength can be used to determine the $H_2O$ column density.

Diagnostic development requires empirical spectral data to establish the sensitivity of the measurements to $H_2O$ concentration,

Presented as Paper 95-0484 at the AIAA 33rd Aerospace Sciences Meeting, Reno, NV, Jan. 9–12, 1995; received Feb. 17, 1995; revision received July 6, 1995; accepted for publication Oct. 3, 1995. 

*Associate Professor, Engineering Division. Member AIAA.
†Principal Scientist, 20 New England Business Center. Member AIAA.
‡Principal Research Scientist, 20 New England Business Center. Member AIAA.
§Principal Research Scientist, 20 New England Business Center.

temperature, wavelength, and bandpass for a range of typical combustion conditions (temperature, pressure, and mole fraction). Although band models based on high-temperature optical measurements have previously been developed for $H_2O$ emission,[13,14] these models are largely empirical in nature and do not provide sufficiently precise a priori predictions of the spectral distributions for use in scramjet reacting flow conditions. Thus, we have performed a series of direct observations of high-temperature $H_2O$ emission spectra behind incident shock waves using a shock tube. Proper application of the shock tube technique provides uniform, well-characterized flowfields containing known, optically thin $H_2O$ concentrations at known temperatures, so that the fundamental emission strengths and spectral signatures can be accurately determined. This effort follows the approach previously described for radiometric measurements of NO concentrations and temperatures.[5,15]

## Experimental Apparatus and Methods

The infrared water emission spectrometer consists of a 12-element HgCdTe array coupled to a 0.35-m monochromator and a folded gold mirror system used to image the flowfield onto the entrance slit of the spectrometer. Image size at the shock tube centerline was $3 \times 3$ and $8.2 \times 8.2$ mm at the near and far edges of the 10.4 cm I.D. tube. The optical path length within the instrument and the path between the spectrometer and the shock tube were purged with dry nitrogen to avoid absorption of the emission signal by water vapor in the room air. Centerline wavelengths for the HgCdTe array elements span from 6.50 to 8.55 $\mu$m with a full width at half maximum (FWHM) bandpass for each element of 0.19 $\mu$m, and calibration measurements have verified that the spectrometer bandpass can be represented by an isosceles triangular shape. The 12 output channels for the spectrometer were synchronously sampled at 125 kHz with 10 bits of resolution. Emission at 9.44 $\mu$m was monitored using a separate, apertured HgCdTe detector equipped with a bandpass filter (0.7 $\mu$m FWHM) and was sampled at 1 MHz also with 10-bit resolution. Absolute calibrations of the spectrometer system and the 9.44-$\mu$m radiometer were performed using a standard NIST traceable radiometric blackbody source.

A 10.4-cm-diam shock tube system,[15] shown schematically in Fig. 1, was used to produce known quantities of water vapor at elevated temperatures (1400–3000 K). Each experiment produced temporally resolved infrared emission from the known $H_2O$ concentration and temperature field behind the incident shock. Two methods were used to produce the high-temperature water vapor mixtures. The first method used carefully prepared dilute stoichiometric mixtures of hydrogen and oxygen in argon. These mixtures react to form water after shock heating to produce a uniform temperature and concentration field behind the incident shock. The second method uses carefully prepared mixtures of water vapor and nitrogen that are shock processed to create a known concentration and temperature radiating system, again behind the incident shock.

## Measurement Results

To calibrate the diagnostic such that the line-of-sight averaged temperature and water number density in an arbitrary flowfield can be measured, the spectral emission of water on a per molecule basis, that will be termed the spectral radiant efficiency, must be known as a function of temperature. The observed spectral radiance in a specified wavelength bandpass $I_\lambda$ [typically in units W/(cm$^2$-sr-$\mu$m)] is a function of the path length $l$, the number density of radiating molecules ($H_2O$), and the spectral radiant efficiency $i_\lambda$ [typically in units W/(molecule-sr-$\mu$m)], as shown in Eq. (1):

$$I_\lambda = \int_0^l i_\lambda[H_2O]\, dl \tag{1}$$

Typically, variations in concentration and temperature along the line of sight are ignored, and the spectral radiance is considered to simply be a product of spectral radiant efficiency, concentration, and path length. The product of the water number density ($H_2O$) and the optical path length $l$ is termed the column density $N_c$, and line-of-sight results are typically parameterized in terms of this product. The path length for the calibration measurements is the diameter of the shock tube, 10.4 cm, and the emission measurement applies equal weighting (in terms of instrument response) to system radiance regardless of position along the path.

The shock tube, as used for calibration purposes, produces precisely controlled path length, water concentration, and temperature such that the observed spectral radiance can be used to determine the spectral radiant efficiency as a function of temperature and wavelength. Boundary-layer effects have been calculated to be small, so that from a calibration perspective nonuniformities along the line of sight are insignificant. Determination of the spectral radiant efficiency $i_\lambda$ in each measurement bandpass is therefore simply a matter of dividing the observed spectral radiance $I_\lambda$ by the known column density for the system $N_c$. A calibration set that shows the variation of spectral radiant efficiency as a function of temperature is therefore produced by varying the temperature behind the incident shock.

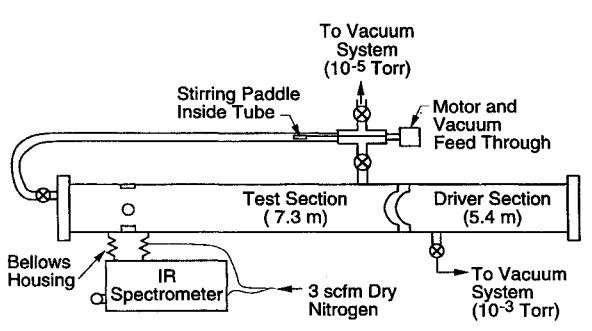


**Fig. 1 Schematic of shock tube apparatus. The mixing tube and motorized stirring system are only used for nonreacting shocks where the initial mixtures contain water vapor.**

### Combustion-Generated $H_2O$

For the combustion-generated $H_2O$ measurements, dilute stoichiometric mixtures of hydrogen and oxygen in argon were shock heated such that the hydrogen and oxygen reacted rapidly behind the incident shock to form water. Mixtures were carefully prepared using ultra-high purity (UHP) gases in clean, initially evacuated (vacuum levels below $5 \times 10^{-5}$ torr) vessels and allowed to cure over several days to ensure that diffusional mixing had created a truly homogenous system. Using this method, the postshock temperature was varied from 1700 to 3000 K at pressures ranging from 4 to 6 atm. Measured shock speed (quantified using time of arrival at discretely spaced high-frequency pressure transducers) and initial fill pressure of the driven section, along with the mole fractions of the hydrogen, oxygen, and argon in the initial mixture, were used as inputs to the shock wave and chemical kinetics modeling code DSHOCK[16] to predict the time history of the reacting gas mixture behind the incident shock. From this calculation, the postshock gas temperature and water concentration were determined as a function of position behind the incident shock.

A detailed hydrogen-oxygen reaction mechanism composed of accepted elementary reactions and rate coefficients from the literature was used to describe the combustion chemistry of the postshock gases. To avoid the complications associated with uncertainties in the elementary chemical reaction rates in the initiation and exponential growth stages of the reaction, only the properties of the reacting mixture well after the passage of the incident shock wave were used to correlate to the emission measurements (i.e., after the chemistry has transitioned into the partial equilibrium regime). Postshock water number density and temperature values were computed using two different sets of elementary reactions and reaction rate coefficients for the hydrogen-oxygen-nitrogen reaction system, one adapted from Warnatz[17] and one given by Miller and Bowman.[18] The two sets gave essentially identical results for the partial equilibrium regime. A boundary-layer correction based on the model of Mirels[19] is included in the DSHOCK calculation; comparison of calculations with and without the boundary-layer correction showed the temperature to increase by no more than 30 K (approximately 1%) and number density to increase by no more than 1% because of the boundary layer in the tube.

Very dilute mixtures of hydrogen and oxygen (hydrogen mole fraction of 5% or less) were used; this ensured partial-equilibrium

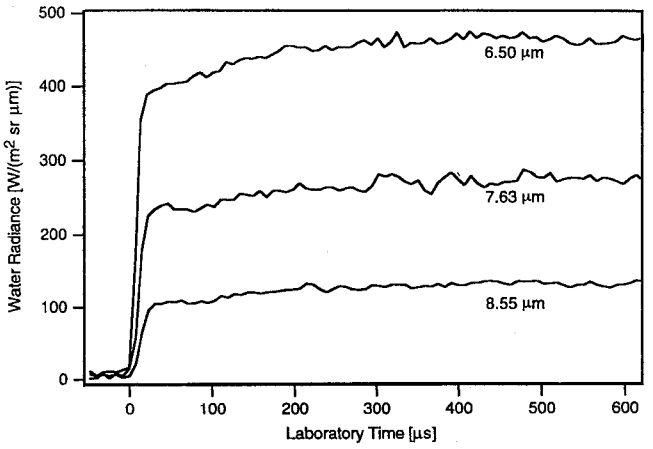


**Fig. 2 Representative time profiles of infrared radiances from $H_2O$ formed in shock-heated $H_2/O_2/Ar$ = 0.032/0.016/0.952 mixture. Postshock conditions are $P$ = 4.9 atm, $T$ = 2420 K, and $H_2O$ = 4.3 × $10^{17}cm^{-3}$.**

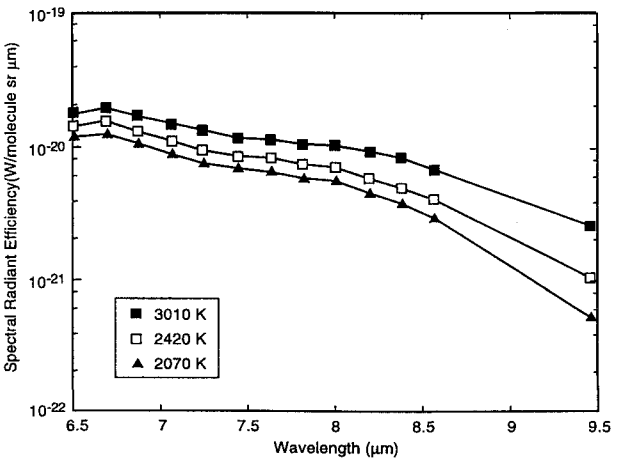


**Fig. 3 Observed spectral distribution for $H_2O$ emission from shock-heated $H_2/O_2/Ar$ mixtures.**

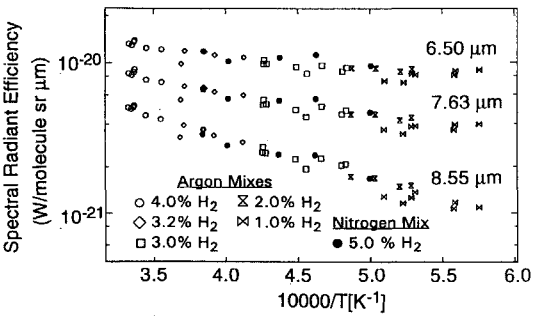


**Fig. 4 Observed spectral radiant efficiencies for combustion-generated $H_2O$ produced by shock-heating stoichiometric mixtures of hydrogen and oxygen in a diluent (argon or nitrogen).**

concentrations of water that were low enough that the postshock mixtures were optically thin for all of the wavelengths in the monitored spectral band. [The determination of criteria for optical thickness is discussed in the section about the spectral band model for $H_2O(\nu_2)$.] Additionally, the dilution of the mixtures minimized the temperature rise associated with the chemical heat release ($\Delta T$ < 300 K). As a result, the uncertainties in predicting the temperature of the reacting mixture were reduced, and detonations were avoided.

Figure 2 shows the water emission at several wavelengths as a function of time after the passage of the incident shock wave. For this case, the initial mixture composition was 3.2% $H_2$, 1.6% $O_2$, and 95.2% Ar. The reflected shock wave arrives at the measurement station at approximately 750 $\mu$s, which signals the end of useful data for this event. Data were averaged over a period of time to reduce the uncertainties in measured radiance levels and the averaging window typically used was between 400 and 600 $\mu$m after the passage of the incident shock wave (in laboratory elapsed time). Over the averaging window, the emission signals in Fig. 2 have a standard deviation of less than 3%, which is typical for the entire calibration data set.

Results of the DSHOCK calculation provide temperature and water concentration in the postshock region. Between 400 and 600 $\mu$s, the computed temperature and water concentration vary by less than 1%, and both quantities are within 2% of their calculated equilibrium values. These results coupled with the data shown in Fig. 2 confirm that the measured emission signal does not vary significantly over the averaging window and that the calculated temperature and water concentration behind the incident shock wave also do not vary significantly over this time period. Thus, the emission measurements from the reacting mixtures can be used with confidence to calibrate the water emission diagnostic.

Observed $H_2O$ emission spectra are shown in Fig. 3 for three different temperatures. Because the wavelengths near 6.5 $\mu$m sample lower vibrational and rotational states, which radiate near the center of the band, the intensity is greatest near 6.5–6.7 $\mu$m. Intensities at longer wavelengths show more variation with temperature since the emission at the longer wavelengths is the result of transitions from higher rotational and vibrational states. This causes a change in the band shape with relative intensity at the longer wavelengths increasing as the temperature rises.

The $H_2O$ spectral radiant efficiency is shown as a function of temperature in Fig. 4. The plot, which shows the emission signal at several wavelengths, includes results from five different $H_2/O_2/Ar$ mixtures. All of the mixtures were stoichiometric mixtures of hydrogen and oxygen; the hydrogen mole friction for each mixture is listed in the legend of Fig. 4. The range of mixtures shown in this figure was carefully chosen to produce an optically thin system with a maximum radiant signal level. Emission data from the various mixtures show excellent agreement over the entire range of temperatures investigated, indicating good consistency in the prepared mixture compositions as well as in the predicted postshock gas compositions.

For the reacting shock experiments, argon was used as the diluent since higher postshock pressures could be achieved than with nitrogen (for fixed driver pressure); thus, emission data with higher signal-to-noise ratio could be obtained with very dilute mixtures [$X(H_2O) < 4\%$]. Some measurements of the water emission from reacting hydrogen-oxygen mixtures with nitrogen as the diluent were also performed. Example data are shown in Fig. 4, illustrating good agreement with the argon data. Typical postshock pressure with nitrogen as the diluent was 1 atm. Good agreement between the two data sets is important since the eventual application of this diagnostic is for measuring the water concentration in the exit plane of an $H_2$/air scramjet test flow where nitrogen will be a major component. Within the uncertainty of the data, there is no observable dependence of the water radiance on the diluent identity (Ar on $N_2$) or on the total pressure (between 1 and 5 atm)—an expected result.

### Shock-Heated $H_2O$

To test the consistency of the combustion-generated $H_2O$ data, manometrically prepared mixtures of water vapor and nitrogen were shock heated directly. The advantage of using the $H_2O/N_2$ mixtures is that, for temperatures below about 2500 K, there is negligible thermal dissociation of $H_2O$, and the postshock mixture temperature and water concentration can be calculated without relying on chemical kinetic modeling. Thus, the kinetics-related uncertainties in determining the postshock conditions are avoided. However, this advantage is offset by the difficulties associated with performing these experiments. Parker et al.[11] have discussed these issues in detail. Briefly, the main difficulty is that when the prepared $H_2O/N_2$ mixture is introduced into the shock tube from the holding tank, some of the water vapor condenses because of the low pressure in the shock tube at the initial stage of the fill process. The condensed water eventually evaporates once the fill process is complete; however, a motorized mixing system must be used to circulate the gas in the driven section to eliminate inhomogeneities in the mixture (see Fig. 1). Typically, several hours elapse between the

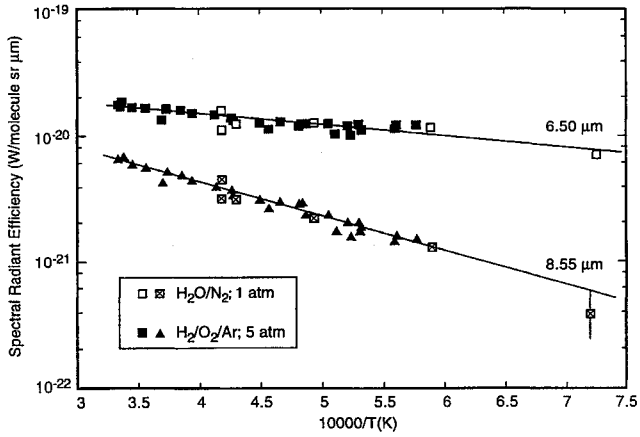


**Fig. 5 Comparison of $H_2O$ spectral radiant efficiencies for $H_2/O_2/Ar$ and $H_2O/N_2$ measurements. The lines represent least-squares fits through the $H_2O_2/N_2/Ar$ data.**

time the fill process is initiated and when the mixture is sufficiently homogenized.

Water radiance as a function of temperature for the $H_2O/N_2$ shocks is plotted in Fig. 5 along with the results of the $H_2/O_2/Ar$ shocks. Nitrogen diluent data were processed similar to the reacting shock data. An average was obtained over an approximate 100-$\mu$s time window, and radiant efficiency was calculated by dividing the observed radiance by the column density calculated using DSHOCK.[16] Here, data are shown for two wavelengths, 6.50 and 8.55 $\mu$m. In the region of overlap, the agreement between the reacting and nonreacting results is very good. By combining the $H_2O/N_2$ and $H_2/O_2/Ar$ data, the temperature range of the radiance calibration extends from 1400 to 3000 K. Also shown in Fig. 5 are least-squares fits to the $H_2/O_2/Ar$ data. The fitting procedure is discussed in detail in the next section.

## Empirical Parameters and Sensitivities

The observed emissions arise from dipole-allowed transitions from a thermally populated upper rotational-vibrational state to a lower rotational-vibrational state. For such transitions, it can be shown[5,20] that the spectral radiant intensity is proportional to the product of a transition probability term that is weakly temperature dependent and a Boltzman population term that is exponential in inverse temperature. Over a limited temperature range and for nearly harmonic oscillators such as $H_2O(\nu_2)$, we expect the intensity at a given wavelength to approximately follow the Arrhenius form:

$$I_\lambda = N_c \alpha_\lambda \exp(-\beta_\lambda / T) \tag{2}$$

where $N_c$ is the product of the water number density and the path length ($H_2O$ column density), and $\alpha_\lambda$ and $\beta_\lambda$ are empirical constants related to the radiative transition probability and the upper state energy, respectively.

To provide convenient parameterizations of the database, we have performed least-squares fits of the observed $I_\lambda/N_c$ (which is $i_\lambda$, the spectral radiant efficiency) values to the form of Eq. (2). The fitting results for the $H_2/O_2/Ar$ data (5 atm) are illustrated in Fig. 6, and the fitting parameters and their standard deviations are tabulated in Table 1. The functional form of Eq. (2) gives good fits to the data at all wavelengths over the 1700–3000 K temperature range of the $H_2/O_2/Ar$ data set. In addition, extrapolations of the fitting functions give excellent agreement with the $H_2O/N_2$ (1 atm) data set down to 1390 K, as shown in Fig. 5. Indeed, inclusion of the $H_2O/N_2$ data in the least-squares analysis does not significantly affect the fitting results. Therefore Eq. (2) with the parameters in Table 1 provides a consistent representation of the wavelength and temperature dependence of optically thin $H_2O$ emission between 6.5 and 9.5 $\mu$m and 1400–3000 K.

The excellent agreement among the $H_2O/N_2$ data at 1 atm, the $H_2/O_2/Ar$ results at 5 atm, and the $H_2/O_2/N_2$ measurements at 1 atm as described earlier confirms several aspects of our analysis. First, as expected, there is no significant pressure or collisional broadening

**Table 1 Fitting parameters for $H_2O$ spectral radiance**

| Wavelength, $\mu$m | $\alpha \times 10^{20}$, W/mol sr $\mu$m[a] | $\beta$, Kelvin[a] |
|---|---|---|
| 6.50 | 3.42 ± 0.27 | 2046 ± 185 |
| 6.69 | 4.55 ± 0.41 | 2556 ± 209 |
| 6.87 | 4.74 ± 0.41 | 3094 ± 204 |
| 7.06 | 4.29 ± 0.50 | 3188 ± 271 |
| 7.24 | 4.00 ± 0.36 | 3444 ± 210 |
| 7.44 | 3.37 ± 0.31 | 3272 ± 217 |
| 7.63 | 3.56 ± 0.32 | 3549 ± 210 |
| 7.81 | 3.57 ± 0.29 | 3765 ± 192 |
| 7.99 | 4.08 ± 0.29 | 4186 ± 168 |
| 8.19 | 4.57 ± 0.42 | 4973 ± 214 |
| 8.37 | 5.27 ± 0.46 | 5678 ± 204 |
| 8.55 | 5.39 ± 0.47 | 6265 ± 203 |
| 9.44[b] | 7.94 ± 0.70 | 10454 ± 390 |

[a]Indicated uncertainties are $\pm 1\sigma$ in the least-squares fit.
[b]9.44 $\mu$m data are fit for $T > 2000$ K only.

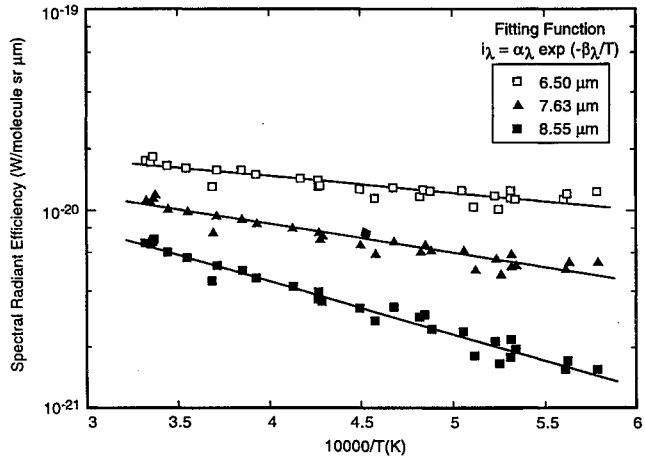


**Fig. 6 Least-squares fits (lines) of spectral radiant efficiencies for $H_2/O_2/Ar$ mixtures.**

effect on the observed optically thin radiances at moderate spectral resolutions. Second, the consistency between the results for the reactive and nonreactive mixtures ($H_2/O_2$ vs direct shock heating of $H_2O$) confirms our approach for determining the combustion-generated $H_2O$ number densities from kinetic modeling calculations of the partial equilibrium state behind the incident shock. Third, as anticipated, the radiances at the longer wavelengths, especially 8.55 and 9.44 $\mu$m, show a much stronger temperature dependence than the radiances at the shorter wavelengths (e.g., 6.50 and 6.69 $\mu$m). Thus radiance ratios (e.g., $I_{6.50\,\mu m}/I_{8.55\,\mu m}$, and $I_{6.50\,\mu m}/I_{9.44\,\mu m}$) can be used as a measurement of temperature. The determined temperature along with the absolute radiance level at a particular wavelength (e.g., 6.50 $\mu$m) can be used to determined the $H_2O$ column density.

The radiance ratio for two wavelengths $\lambda_i$ and $\lambda_j$ has the form

$$R_{ij} = A_{ij} \exp(B_{ij}/T) \tag{3}$$

where $A_{ij} = \alpha_i/\alpha_j$ and $B_{ij} = \beta_j - \beta_i$. The quantities $A_{ij}$ and $B_{ij}$ can be determined from the fitting parameters in Table 1; however, this procedure incorporates uncertainties in the absolute radiance and water number density determinations that are eliminated by the ratiometric method. More precise determinations of $A_{ij}$ and $B_{ij}$ are given by least-squares fitting of the specific experimental $R_{ij}$ values using Eq. (3), as illustrated for three wavelength pairs in Fig. 7.

The accuracy to which temperature and column density can be determined from the empirical fitting functions can be estimated by propagation of errors in Eqs. (2) and (3). Rearrangement of Eq. (3) to determine temperature from the ratio of the intensities at wavelengths $\lambda_i$ and $\lambda_j$ gives

$$T = \frac{B_{ij}}{\ell n(R_{ij}/A_{ij})} \tag{4}$$

The relative error in $T$, $\delta T/T$, is then given by the square root of the sum of the squares of the relative errors of the numerator and denominator, resulting in a function of the measurement error $\delta R$ and the statistical fitting uncertainties $\delta B$ and $\delta A$. Expression of these errors as standard deviations then gives the standard deviation in $T$. Differentiation of Eq. (4) gives the following:

$$\delta T/T = (T/B_{ij})\left[(\delta B_{ij}/T)^2 + (\delta R_{ij}/R_{ij})^2 + (\delta A_{ij}/A_{ij})^2\right]^{\frac{1}{2}} \quad (5)$$

The values of $\delta A/A$ and $\delta B/B$ are determined from the standard deviations in the least-squares fits to $\ell_n(R)$ vs $1/T$ for a given wavelength pair and are typically 3–6% for the data described earlier. The measurement uncertainty of the radiance ratio, $\delta R/R$, is simply given by the square root of the sum of the squares of the individual radiance measurement uncertainties at the two wavelengths and thus depends upon the signal/noise ratio and the instrument calibration accuracy at each wavelength. Typically the temperature determination employs a short wavelength such as 6.50 to 6.69 $\mu$m, for which the fractional measurement uncertainty is between 0.03 and 0.015, and a long wavelength such as 8.55 or 9.44 $\mu$m, for which the measurement uncertainty (due to decreased signal/noise ratio) can be as poor as 0.10. Thus the relative uncertainty in the radiance ratio, $\delta R/R$, is dominated by the measurement uncertainty at the longer wavelength. In practice, this wavelength can be chosen so that $\delta R/R \leq 0.1$.

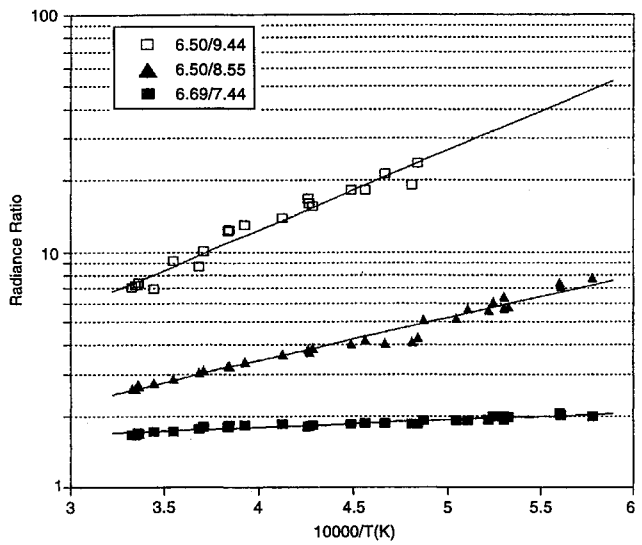


**Fig. 7 Observed radiance ratios for the wavelength pairs indicated. The lines represent least-squares fits to the data.**

Values of $\delta T/T$, calculated from Eq. (5) for the wavelength pairs 6.50/9.44, 6.50/8.55, and 6.69/8.55 $\mu$m and assuming $\delta R/R = 0.1$, are plotted in Fig. 8. Values for intensity ratios using 6.50 and 9.44 $\mu$m are limited to temperatures above 2000 K, where the 9.44-$\mu$m radiometer gives acceptable signal/noise ratios for column densities less than $10^{19}$ molecules/cm$^2$. Inspection of Eq. (5) illustrates that the relative temperature error increases with temperature and that accuracy is increased as the value of $B_{ij}$ becomes larger. Values for $B_{ij}$ typically can be maximized by using widely spaced wavelengths. This approach is tempered because, at the longer, more temperature-sensitive wavelengths, the signal-to-noise ratios may become unacceptably large. Hence a balance between signal-to-noise ratio and increased temperature sensitivity must be achieved for each application. Based on preliminary shock tunnel exit plane radiance measurements for the facility at Physical Sciences, Inc.,[12] and the fluctuations in the observed signal levels, measurements at the combustor exit plane for $H_2O$ radiances with an accuracy of $\delta I/I$ of 0.03–0.1 giving $\delta R/R \approx 0.1$ can be expected. Hence, the relative error in the measured temperature will be less than 10% and perhaps as low as 5% in some cases.

The expected uncertainties in the measured $H_2O$ column densities can be determined in a similar fashion. Rearrangement of Eq. (2) gives the column density $N_c$:

$$N_c = \frac{I_\lambda}{\alpha_\lambda \exp[-(\beta_\lambda/T)]} \quad (6)$$

The relative error in the column density is then

$$\delta N/N = \left\{(\delta I/I)^2 + (\delta\alpha/\alpha)^2 + (\beta^2/T^2)\left[(\delta\beta/\beta)^2 + (\delta T/T)^2\right]\right\}^{\frac{1}{2}} \quad (7)$$

In this case, the relative error $\delta N/N$ is primarily determined by the relative errors in $\alpha_\lambda$ and in the measured radiance. The additional temperature-dependent contribution from errors in $\beta$ and $T$ is minimized by using the wavelengths with small values of $\beta_\lambda$, e.g., 6.50 or 6.69 $\mu$m. The dependence of $\delta N/N$ on temperature is plotted in Fig. 9 for $\lambda = 6.50\,\mu$m, assuming $\delta I/I = 0.03$ and using the $\delta T/T$ values for the wavelength pairs from Fig. 8. The error in column density is limited by the uncertainty in $\alpha_\lambda$ at high temperatures and uncertainties in temperature and $\beta$ increase the relative column density error at low temperature. Based on these results, we expect

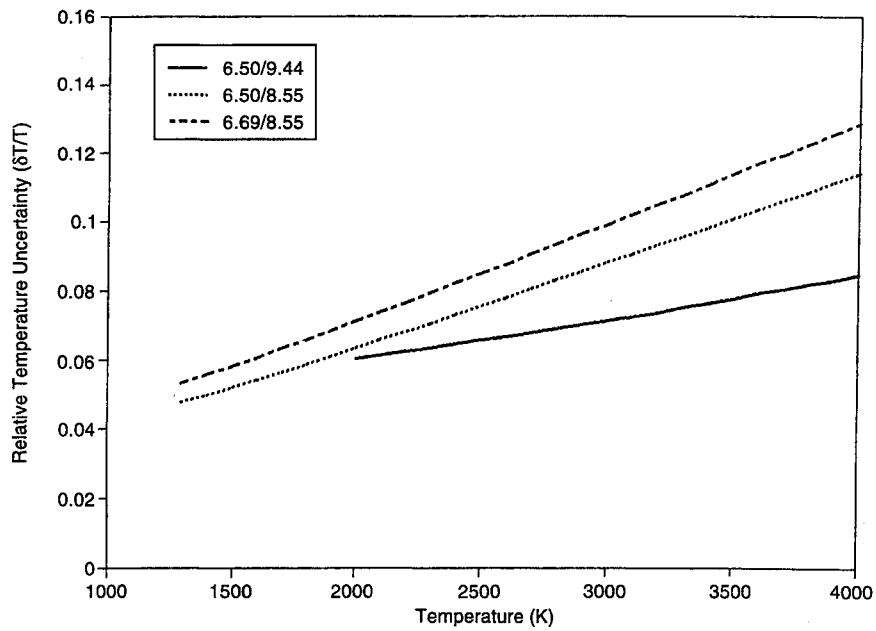


**Fig. 8 Uncertainty in measured exit plane $H_2O$ temperatures using the ratiometric method, assuming $\delta R/R = 0.10$.**

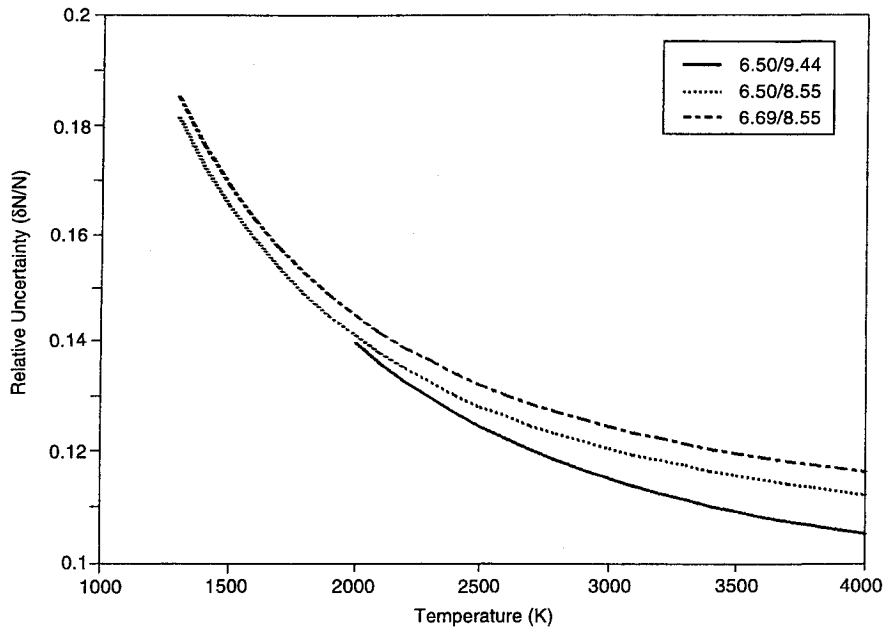


**Fig. 9 Uncertainty in the exit plane $H_2O$ column densities measured using radiance at 6.5 $\mu$m, assuming $\delta R/R = 0.10$ and $\delta I/I = 0.03$.**

to determine combustor exit plane column densities with relative errors of less than 20%.

## Spectral Band Model for $H_2O(\nu_2)$

To aid in interpretation of the high-temperature radiance data, it is important to compare the experimental results with predicted dependencies of the emission intensity on wavelength, temperature, and water number density. However, such predictions are difficult, because there are no well-validated, line-by-line spectroscopic descriptions of $H_2O$ infrared emission at combustion temperatures.

One must remember that, for the measurement discussed in this paper, the observed radiance is the sum of the radiance contributed by each individual line as dictated by the thermally populated number density of each rotational-vibrational state. In the case of this measurement, the bandpass for the spectrometer is 0.19 $\mu$m, compared with a typical linewidth of 0.0003 $\mu$m for water in this spectral region. One can easily see that the radiance observed by the spectrometer originates from literally hundreds of lines. However, detailed examination of the water spectra at temperatures of 1500 K and less and at pressures of approximately 1 atm, using the Air Force HITRAN database,[21,22] reveals that the line density is not sufficient to produce a continuum-like spectrum. This has profound implications in terms of the optical thickness of the measurement. Radiation measurements of continuum systems can use the value of emissivity to track the effect of optical thickness (a system is considered to be thick for emissivities greater than 0.2–0.3). For very structured spectra, however, this technique will not work since an average value of emissivity over a bandpass does not take into account the structure within the band. For instance, 80% of the radiance observed may originate in 20% of the band. This implies that local wavelength regions may be optically thick in spite of a relatively low average emissivity value for the total wavelength bandpass. To set column density values that are known to be optically thin over the entire bandpass, a line-by-line examination of the water spectra using the HITRAN database[21,22] was performed to define the maximum line strength within each bandpass. This database is incomplete but includes the highly populated and strong transitions (tabulated for 297 K and 1 atm pressure) so that a maximum line strength for each bandpass can be estimated. This line strength, which was identified using the HITRAN database[21,22] and adjustments for temperature effects,[21] is then used to define a column density that will produce an emissivity of 0.3 at line center (this value was used in this work as an upper bound for an optically thin system). Since the strongest transition was chosen and inspection of the database shows that the strong transitions are reasonably well separated, this criterion for optically thin should be quite conservative. As an added note, in spite of the incompleteness of the HITRAN database,[21,22] the vibrational levels included in the database (levels 3 and below) are dominantly populated at temperatures of 3000 K and below.[11] These column density values were used to set upper bound values for the shock tube calibration experiments.

Data comparison between experimental groups is always important when developing a diagnostic such as the one discussed in this paper, and results from a band model for water developed for the rocket plume community provide an excellent opportunity for this comparison. Comparisons with integrated results from the HITRAN database consistently underpredicted experimental radiance levels (particularly for wavelengths greater than 7.5 $\mu$m). Therefore, the band model that appears in the Air Force SIRRM plume radiation code, described by Ludwig et al.[23] and based on a comprehensive series of long path flame measurements, was used. Note that the experimental data upon which the band model is based were almost exclusively obtained at optically thick conditions and then processed to account for the effect of self-absorption.

The functional form of the band model is derived assuming a random distribution of collision-broadened lines with an exponential distribution of line intensities. In this case the emissivity $\varepsilon$ at transition frequency $\nu$ is given by

$$\varepsilon = 1 - \exp\left[ - \frac{k(\nu)u}{\{1 + [k(\nu)u/4a(\nu)]\}^{\frac{1}{2}}} \right] \tag{8}$$

where $k(\nu)$ is the effective absorption coefficient at standard temperature and pressure (STP) in centimeter$^{-1}$ atmosphere$^{-1}$, $u$ is the optical depth at STP in centimeter-atmosphere (partial pressure of $H_2O$ × path length $\times 273/T$), and $a(\nu)$ is the ratio of the collision-broadened line width $\gamma_c$ to the line spacing parameter $d(\nu)$. The collision line width is $\gamma_c$ determined by the sum over species partial pressures and collision-broadening parameters as reported by Ludwig.[13] The function in Eq. (8) was fit to the flame spectral emission data to determine empirically the values for $k(\nu)$ and $d(\nu)$; these values are tabulated in Ludwig's paper,[13] the SIRRM code,[23] and Ref. 24.

Using these tabulated values, Eq. (8) has been evaluated for the 5–9 $\mu$m spectral region. As expected, for the range of experimental conditions in the shock calibrations, the nonlinear term in the denominator of Eq. (8) is negligible, and the values for $k(\nu)$ are small enough that the predicted radiance scales linearly with ($H_2O$). Predicted spectral distributions for 2000 and 3000 K are

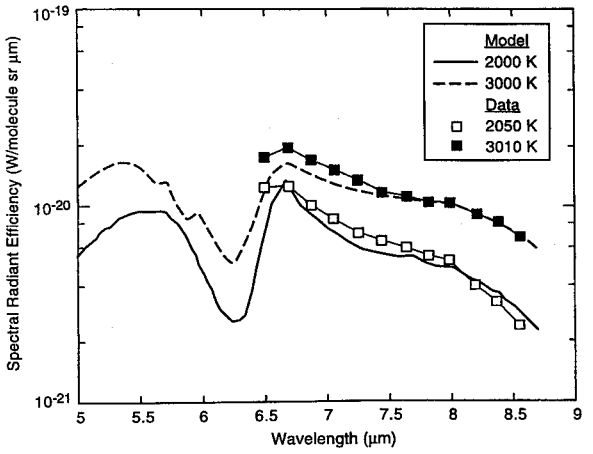


**Fig. 10 Comparison of shock tube spectra to band model predictions.**

compared with the observed radiance in Fig. 10. In general, the agreement between model and data is quite good, with the model predictions falling within 20% of the data for all wavelengths except 6.50 $\mu$m.

We have also used the band model approach to evaluate the effects of optical thickness on the diagnostic and its application. If the observed column density is large enough, a significant fraction of the emitted intensity is reabsorbed, and the medium is said to be optically thick. Under these conditions, the observed intensity is less than that expected from linear scaling with $H_2O$ column density [Eq. (1)]. Although the shock tube measurements reported here were configured to achieve optically thin conditions, combustor exit plane measurements may sample larger $H_2O$ column densities and approach optically thick conditions, necessitating a correction of the observed intensities.

Since the onset of optical thickness depends on the number density of species in the lower state of the transition, the effect tends to be most pronounced for transitions terminating in the ground vibrational state, i.e., near the center of the band. As shown previously,[11] the strongest rotational lines terminating in the ground vibrational state can be quite sensitive to self-absorption even at $H_2O$ column densities as low as $10^{18}$ molecules-cm$^{-2}$. However, when the intensity is spread across the 0.19-$\mu$m bandpass of the array monochromator, hundreds of lines of varying strengths are sampled and the threshold for significant attenuation of the intensity is higher than that for a single strong line.

The SIRRM radiation code[23] has been used to evaluate optical thickness effects more quantitatively. These calculations employ the Ludwig[13] empirical band model described earlier to account for sublinear scaling of intensity with column density. Calculations are performed as a function of temperature, pressure, and column density for the actual detector wavelengths and bandpasses used in the measurements. Figure 11 illustrates results from these calculations that have been parameterized to predict the column density at which 10% self-absorption will occur as a function of temperature for a range of pressures. As shown in Fig. 11, at 1500 K an almost linear relationship between threshold column density and pressure exists compared with a vanishingly small pressure dependence at 3000 K and above. Explanation of this behavior is simply that at the low temperatures the measurement is approximating the emission from a set of isolated lines where pressure broadening controls the optical thickness at the line center. In this limit, threshold column density will scale linearly with pressure. At higher temperatures, more states become populated and the lower energy states become less dominantly populated. In a sense, the spectrum fills in and becomes, on average, less structured. The limit for this behavior is an unstructured spectrum similar to that for gray body radiators such as particulate. In this limit, pressure has no effect, and an optical cross section $\sigma_\lambda$ for the system may be computed. Equation (9) is the optically thin radiance based upon a cross section, and comparison with Eq. (1) reveals that optical cross section is equal to the spectral radiant efficiency divided by the blackbody radiance $N_{\lambda,bb}$, Eq. (10). The importance of the optical cross

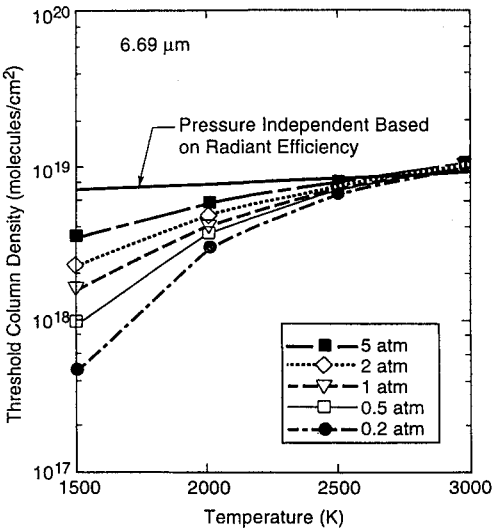


**Fig. 11 Threshold column density for 10% self-absorption as a function of temperature at a wavelength 6.69 $\mu$m. The pressure-independent solution is based on a cross section calculated using data from this work.**

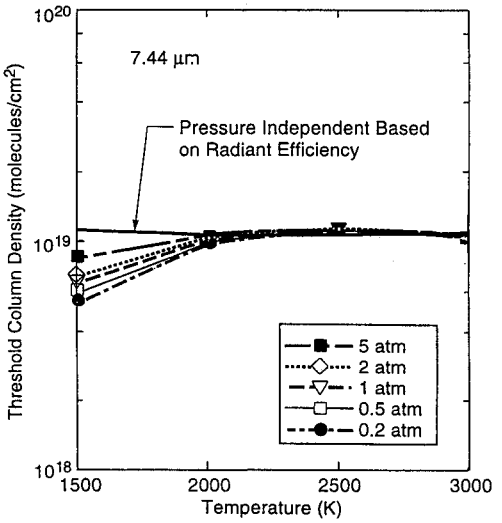


**Fig. 12 Threshold column density for 10% self-absorption as a function of temperature at a wavelength 7.44 $\mu$m. The pressure-independent solution is based on a cross section calculated using data from this work.**

section is that, when it is appropriate to use, the radiance from an optically thick system becomes very simple to calculate as shown by Eq. (11):

$$I_\lambda = N_c \sigma_\lambda N_{\lambda,bb} \tag{9}$$

$$\sigma_\lambda = i_\lambda / N_{\lambda,bb} \tag{10}$$

$$I_\lambda = (1 - \exp^{-N_c \sigma_\lambda}) N_{\lambda,bb} \tag{11}$$

Included in Fig. 11 is the computed threshold column density calculated using the cross section derived from the spectral radiant efficiencies produced by this work. As one can see, as the temperature increases, the specific pressure curves calculated with SIRRM asymptote to the single curve defined by the optical cross section. This not only shows that the system becomes pressure insensitive but also illustrates the good agreement between the two data sets.

Figure 12 is a similar plot for a longer wavelength, 7.44 $\mu$m. As this plot shows the pressure dependence is much weaker with virtually no pressure dependence for temperature of 2000 K and above. This plot also includes the threshold column density calculated from the spectral radiant efficiency, and within the accuracy of the two

databases, agreement is excellent. Significantly less pressure dependence exists at this wavelength than at 6.69 since the longer wavelengths are less dominated by ground state transitions. Further examination of the SIRRM calculations shows that, at 8.55 $\mu$m, virtually no pressure dependence of threshold column density exists for temperatures of 1500 K and above.

Finally, the effect of optical thickness on the measured temperature must be quantified. Clearly, the result shown in Figs. 11 and 12 indicate that self-absorption because of high column densities complicates the interpretation of the data but that an accurate measure of column density can still be achieved. In the case of temperature, the development within this paper explicitly assumed an optically thin system to produce a simple temperature measurement methodology based on the ratio of signals at two wavelength. Examination of the error induced in the temperature measurement when the column density is at the 10% self-absorption level indicated that the error in temperature because of the self-absorption was 6% or less.

Figures 11 and 12 illustrate that when applying this type of measurement to a system, the expected column densities and temperatures must be carefully considered. For temperatures of 1500 K and above at pressures greater than 1 atm, column densities of $1.5 \times 10^{18}$ mol/cm$^2$ or less will be optically thin. In instances where column densities may be larger than this value, longer detection wavelengths such as 7.44 $\mu$m rather 6.69 $\mu$m may be used. Finally, using longer wavelengths has the added advantage that for most pressures and temperatures of interest, the spectral radiant efficiency can be replaced by the optical cross section since pressure-dependent effects become insignificant. This formulation allows direct determination of the number density and temperature in a manner that includes the effects of self-absorption.

## Conclusions

A comprehensive set of spectral radiance efficiencies for the wavelengths 6.50–9.44 $\mu$m, temperatures of 1400–3000 K, and pressures of 1–5 atm has been produced for water emission. These data were carefully produced using a shock tube coupled to an infrared spectrometer and a single bandpass radiometer. The database defines a set of empirical calibration functions that permits quantitative determinations of temperatures and path-integrated $H_2O$ column densities from spectral radiance measurements in a supersonic $H_2$/air combustor or other high-temperature water-laden flows. Based on the statistical uncertainties in the data, the expected accuracy for the nonintrusive measurements are 5–10% for temperature and 10–20% for $H_2O$ column density. A high-temperature spectral band model has also been used to compare experimental and predicted spectral radiance (agreement was excellent) and to examine the effects of optical thickness on the implementation of this diagnostic. The threshold column density for self-absorption was found to be approximately $1.5 \times 10^{18}$ mol/cm$^2$ for temperatures of 1500 K and above and pressures greater than 1 atm at 6.5 $\mu$m. At wavelengths of 7.44 $\mu$m and above, the threshold for 10% self-absorption is approximately $10^{19}$ mol/cm$^2$ for temperatures greater than 2000 K and pressures greater than 0.2 atm. In addition, at longer wavelengths and higher temperatures, radiance from water can be modeled as a gray body radiator with the optical cross section calculated as the spectral radiant efficiency divided by the blackbody radiance for the wavelength in question. This approximation is valid for temperatures greater than 2000 K at wavelengths greater than or equal to 7.44 $\mu$m. Use of the optical cross section allows self-absorption effects to be included explicitly rather than as a correction to optically thin analysis. The multiwavelength approach offered by the infrared array spectrometer permits selection of wavelength combinations that mitigate optical thickness effects and optimize sensitivity to temperature and column density. This emission diagnostic therefore can be used to accurately quantify temperature and $H_2O$ column density for a range of high-temperature flows in a variety of facilities.

## Acknowledgments

This work was supported by the National Aerospace Plane Joint Program Office; Kervyn Mach, technical monitor.

## References

[1]Parker, T. E., Allen, M. G., Reinecke, W. G., Legner, H. H., Foutter, R. R., and Rawlins, W. T., "High Temperature Supersonic Combustion Testing with Optical Diagnostics," *Journal of Propulsion and Power*, Vol. 9, No. 3, 1993, pp. 486–492.

[2]Allen, M. G., Parker, T. E., Reinecke, W. G., Legner, H. H., Foutter, R. R., Rawlins, W. T., and Davis, S. J., "Fluorescence Imaging of OH and NO in a Model Supersonic Combustor," *AIAA Journal*, Vol. 31, No. 3, 1993, pp. 505–512.

[3]Parker, T. E., Allen, M. G., Foutter, R. R., Reinecke, W. G., Legner, H. H., Davis, S. J., and Rawlins, W. T., "An Experimental Study of Supersonic $H_2$-Air Combustion in a Shock Tunnel Flow Facility," *24th Symposium (International) on Combustion*, Combustion Inst., Pittsburgh, PA, 1992, pp. 1613–1620.

[4]McMillin, B. K., Palmer, J. L., Seitzman, J. M., and Hanson, R. K., "Two-Line Instantaneous Temperature Imaging of NO in a Scramjet Model Flowfield," AIAA Paper 93-0044, Jan. 1993.

[5]Rawlins, W. T., Parker, T. E., Foutter, R. R., and Allen, M. G., "Time-Resolved Infrared Emission Spectroscopy in High-Enthalpy Supersonic Air Flows," *AIAA Journal*, Vol. 31, No. 3, 1993, pp. 499–504.

[6]Meijer, G., and ter Meulen, J. J., "Sensitive Quantum State Selective Detection of $H_2O$ and $D_2O$ by (2 + 1) Resonance Enhanced Multiphoton Ionization," *Journal of Chemical Physics*, Vol. 85, No. 12, 1986, pp. 6914–6922.

[7]Docker, M. P., Hodgeson, A., and Simons, J. P., "Molecular Emission from $H_2O/D_2O$ $C^1B_1$ and Photodissociation Dynamics of a $B^1A_1$ Surface," *Molecular Physics*, Vol. 57, No. 1, 1986, pp. 129–147.

[8]Engel, V., Meijer, G., Bath, A., Andersen, P., and Schinke, R., "The C-A Emission in Water: Theory and Experiment," *Journal of Chemical Physics*, Vol. 87, No. 8, 1987, pp. 4310–4314.

[9]Allen, M. G., Davis, S. J., Kessler, W. J., Palombo, D. A., and Sonnenfroh, D. M., "Diode Laser Instrumentation for Aeropropulsion Applications," AIAA Paper 95-0427, Jan. 1995.

[10]Baer, D. S., Nagali, V., Furlong, E. R., and Hanson, R. K., "Scanned- and Fixed-Wavelength Absorption Diagnostics for Combustion Measurements Using a Multiplexed Diode-Laser Sensor System," AIAA Paper 95-0426, Jan. 1995.

[11]Parker, T. E., McManus, K. R., Blair, D. M., Foutter, R. R., and Rawlins, W. T., "Exit Plane Water Measurement in Scramjet Flows," AIAA Paper 94-0387, Jan. 1994.

[12]Parker, T. E., Allen, M. G., Foutter, R. R., Sonnenfroh, D. M., and Rawlins, W. T., "Measurements of OH and $H_2O$ for Wall and Axial Injection in a Scramjet Combustor," *Journal of Propulsion and Power*, Vol. 11, No. 6, 1995, pp. 1154–1161.

[13]Ludwig, C. B., "Measurements of the Curves-of-Growth of Hot Water Vapor," *Applied Optics*, Vol. 10, No. 5, 1971, pp. 1057–1073.

[14]Von Rosenberg, C. W., Jr., Pratt, N. H., and Bray, K. N. C., "Absolute $H_2O$ $\nu_2$-Band Intensity Obtained from Reacting $H_2 + O_2$ Mixtures Behind Shock Waves," *Journal of Quantitative Spectroscopy and Radiative Transfer*, Vol. 10, No. 11, 1970, pp. 1155–1169.

[15]Rawlins, W. T., Foutter, R. R., and Parker, T. E., "Vibrational Band Strengths and Temperatures of Nitric Oxide by Time-Resolved Infrared Emission Spectroscopy in a Shock Tube," *Journal of Quantitative Spectroscopy and Radiative Transfer*, Vol. 49, No. 4, 1993, pp. 423–431.

[16]Mitchell, R. E., and Kee, R. J., "A General-Purpose Computer Code for Predicting Chemical Behavior Behind Incident and Reflected Shocks," Sandia National Labs., SAND82-8205, Livermore, CA, Feb. 1991.

[17]Warnatz, J., "Rate Coefficients in the C/H/O System," *Combustion Chemistry*, edited by W. C. Gardiner Jr., Springer–Verlag, New York, 1984, pp. 197–360.

[18]Miller, J. A., and Bowman, C. T., "Mechanism and Modeling of Nitrogen Chemistry in Combustion," *Progress in Energy and Combustion Science*, Vol. 15, No. 4, 1989, pp. 287–338.

[19]Mirels, H., "Test Time in Low-Pressure Shock Tubes," *Physics of Fluids*, Vol. 6, No. 9, 1963, pp. 1201–1213.

[20]Herzberg, G., *Molecular Spectra and Molecular Structure: I. Spectra of Diatomic Molecules*, Van Nostrand, New York, 1950, pp. 20, 124–128.

[21]Killinger, D. K., and Wilcox, W. E., "USF Hitran-PC," Version 2.2, Center for Laser Atmospheric Sensing, Dept. of Physics, Univ. of South Florida, Tampa, FL, Aug. 1993.

[22]Rothman, L. S., Gamache, R. R., Goldman, A., Brown, L. R., Toth, R. A., Pickett, H. M., Poynter, R. L., Flaud, J. M., Camy-Peyret, C., Barbe, A., Husson, N., Rinsland, C. P., and Smith, M. A. H., "The HITRAN Database: 1986 Edition," *Applied Optics*, Vol. 26, No. 19, 1987, pp. 4058–4097.

[23]Ludwig, C. B., Malkmus, W., Walker, J., Freeman, G. N., Reed, R., and Slack, M., "Standardized Infrared Radiation Model (SIRRM), Volume 1: Development and Validation," U.S. Air Force Rocket Propulsion Lab., AFRPL-TR-81-54, Edwards AFB, CA, Aug. 1981.

[24]Ludwig, C. B., Malkmus, W., Reardon, J. E., and Thompson, J. A. L., "Handbook of Infrared Radiation from Combustion Gases," NASA SP-3080, 1973.